Met. Mater. Int., Vol. 23, No. 6 (2017), pp. 1188~1196
doi: 10.1007/s12540-017-7111-0

SHS Synthesis of Si-SiC Composite Powders Using Mg and Reactants From Industrial Waste

Tawat Chanadee[1,2,*]

[1]Department of Materials Science and Technology, Faculty of Science, Prince of Songkla University, Songkhla, 90110, Thailand
[2]Ceramic and Composite Materials Engineering Research Group (CMERG), Center of Excellence in Materials Engineering (CEME), Prince of Songkla University, Songkhla, 90110, Thailand

(received date: 9 February 2017 / accepted date: 12 April 2017)

Si-SiC composite powders were synthesized by self-propagating high-temperature synthesis (SHS) using reactants of fly ash-based silica, sawdust-based activated carbon, and magnesium. Fly ash-based silica and sawdust-based activated carbon were prepared from coal mining fly ash and Para rubber-wood sawdust, respectively. The work investigated the effects of the synthesis atmosphere (air and Ar) on the phase and morphology of the SHS products. The SHS product was leached by a two-step acid leaching processes, to obtain the Si-SiC composite powder. The SHS product and SHS product after leaching were characterized by X-ray diffractometry, scanning electron microscopy and energy dispersive X-ray spectrometry. The results indicated that the SHS product synthesized in air consisted of Si, SiC, MgO, and intermediate phases (SiO_2, Mg, Mg_2SiO_4, Mg_2Si), whereas the SHS product synthesized in Ar consisted of Si, SiC, MgO and a little Mg_2SiO_4. The SiC content in the leached-SHS product was higher when Ar was used as the synthesis atmosphere. As well as affecting the purity, the synthesis atmospheres also affected the average crystalline sizes of the products. The crystalline size of the product synthesized in Ar was smaller than that of the product synthesized in air. All of the results showed that fly ash and sawdust could be effective waste-material reactants for the synthesis of Si-SiC composite powders.

Keywords: composites, self-propagating synthesis, crystallization, phase transformation, X-ray diffraction

1. INTRODUCTION

Silicon carbide (SiC) is a non-oxide ceramic with outstanding mechanical, physical and thermal properties. Its high mechanical strength and hardness, high thermal conductivity and thermal shock resistance, low thermal expansion coefficient, low density, excellent oxidation and corrosion resistance [1,2] make it ideal for many industrial applications.

The production of high density SiC by solid state sintering is difficult due to the strong covalent bond between Si and C. Therefore, typically, dense SiC is obtained by hot pressing with the addition of a finely-pulverized covalent substance like Si, because Si exhibit good bonding with SiC [3].

The production of SiC is based on carbothermal reduction of SiO_2 by coke known as the Acheson process. However, due to the high reaction temperatures and long reaction time of the process, the product contains large grains and is invariably contaminated with more or less oxygen [1,2]. Alternative methods of SHS such as sol-gel, mechanical milling, thermal plasma, microwave and laser synthesis have been reported [4] but those methods have very high operating costs and complicated processes with expensive precursors and equipment [4].

Nonetheless, self-propagating high temperature synthesis has been considered an economical way to produce fine SiC powders by using the high temperature exothermic reaction of specific materials. It is a very uncomplicated, energy-efficient method because a high temperature furnace and a large energy input are not required. Although, SiC can be synthesized by SHS using elemental silicon and carbon [5], the enthalpy of reaction between Si and C is too low (75 $kJ \cdot mol^{-1}$) [6] and temperature produced is not stable enough for an efficient reaction. Hence, SHS of Si and C for SiC does not work. Previous work by Chanadee and Niyomwas [7] has reported the possibility of synthesizing Si-SiC composite from the reactant mixture of SiO_2 and C using Mg in the reduction process of the SiO_2. Pure Si-SiC was obtained after the as-synthesized product was leached by an acid solution.

In recent years, waste materials, like fly ash and wood sawdust from mining and wood manufacturing industries, have been favored as sources of SiO_2 and carbon for synthesizing

*Corresponding author: tawat.ch@psu.ac.th

SiC and SiC composite [8-14].

This study of the self-propagating high temperature synthesis of Si-SiC composite powder from low cost reactant materials include an investigation of the influence of synthesis atmosphere on the phase and morphology of the SHS products. Interestingly, these synthesized composite powders do not require sintering aid in further hot pressing typically necessary in the production of SiC.

2. EXPERIMENTAL PROCEDURE

2.1. Preparation of fly ash-based silica (FA-based silica)

Fly ash can be classified by ASTM C-618 standard into class F or C based on the total content of SiO_2+Al_2O_3+Fe_2O_3. When the sum is in the range of 50%-70%, the fly ash is classified as class C. If the sum is greater than 70%, it is classified as class F [24]. In this work, raw fly ash (Fa, class C) was received from Mae Moh mine, Lampang, Thailand. It was washed with distilled water in order to eliminate soluble inorganics then, heated at 110 °C for 24 h in an oven. Hydrochloric acid (HCl: 98%, 1.84 $g \cdot mL^{-1}$) was used as the leaching medium. Desired concentrations of HCl were prepared by dilution with de-ionized water (DI water).

A 10 g of FA was stirred in 60 mL HCl solution at concentrations of 1, 3, and 5 M (labeled at FA-1, FA-3, and FA-5, respectively). The solution was stirred in a covered beaker for 3 h at a constant heat of 80 °C. After that, the leached-FA residue was separated from the solution by filtering through filter paper, assisted with a pump inlet. Using hot water, the pH of the leached-FA residue was adjusted to 7.0 by several washs. The neutralized FA residue was dried at 80 °C for 24 h, then, heated at 1,000 °C for 2 h to activate the reaction surface to produce the experimental fly ash-based silica powders. The oxide compositions contained in the raw fly ash and the experimental silica powder from fly ash were examined by X-ray fluorescence (XRF, PW2004, PHILIPS, the Netherlands).

2.2. Preparation of sawdust-based activated carbon (SD-based activated carbon)

The caboneceous precursor for the preparation of the activated carbon was raw Para-rubbber wood-sawdust (SD) from a sawmill in Raman, Yala, Thailand. The raw sawdust was washed and dried at 80 °C for 24 h then, sieved to obtain uniformly-sized particles.

Potassium carbonate (K_2CO_3) dissolved in DI water at a ratio of 10 g : 100 mL was used for the activating process. 10 g of dried-and cleaned SD was impregnated with 100 mL of the K_2CO_3 solution. The mixture was heated at 80 °C under a minimum magnetic stirring until completely dry and put in an oven at 110 °C for 24 h. Four samples of the obtained oven-dried material were put into crucibles and then separately placed in a muffle furnace (LENTON, UAF 16/10/2416 CG), where they were heated to 500 °C by increment of 10 $°C \cdot min^{-1}$ [15-17] and held at this temperature for 1, 3, 5, and 8 h under air atmosphere, being labelled as SD-1, SD-3, SD-5 and SD-8, respectively. The resulting carbon powders were washed to remove all remaining chemical agents, adjusted to neutral pH with DI water and finally dried at 80 °C for 24 h to produce sawdust-based activated carbon powder. The C, H, and N/O elements of the raw sawdust and the activated carbon from the raw sawdust were analysed by an elemental analyzer (CHNS-O, Flash EA 1112, Thermo quest, Italy).

2.3. Synthesis and characterization of Si-SiC composite powders

FA-5 (SiO_2), SD-3 (activated C) and magnesium (Mg, Riedel-deHaen, 99%) powders (listed as FA-5/SD-3/Mg) were used as reactants.

The overall chemical reaction for synthesizing the Si-SiC composite used in this work is expressed in reaction (1).

$$2SiO_{2(s)} + C_{(s)} + 4Mg_{(s)} \rightarrow Si_{(s)} + SiC_{(s)} + 4MgO_{(s)};$$
$$T_{ad} = 2{,}162.7\ °C,\ \Delta H = -655.15\ kJ \cdot mol^{-1} \quad (1)$$

In this study, 6.88 g of FA-5 was combined with 0.34 g of SD-3 and 2.78 g of magnesium. The products synthesized in air and Ar after SHS reaction and after leaching were 5.89 g, 1.03 g, 4.58 g, and 1.10 g, respectively. The products synthesized in air and Ar after leaching contained SiC 14.72% and 53.31%, as shown in Table 3.

The reaction mechanisms to form Si-SiC composite were explained in previous works [18-20]. In combustion synthesis, adiabatic temperature (T_{ad}) is important in predicting the reaction of the reactants and also the occurence of the self-propagated reaction. Therefore, theoretically, T_{ad} can be calculated from the enthalpy of reaction (ΔH) reported by Moore and Feng [21] adapted with HSC® chemistry v.5.1-aided software.

The calculated T_{ad} of the reaction (1) was lower than 2,200 °C which would result in a slow and incomplete SHS reaction [22]. Hence, 3 g powder mixture of aluminium (Al, Himedia Laboratories, 93%) and iron oxide (Riedel-deHaen, 97%) with a molar ratio of 1 : 2 (Fe_2O_3 : 2Al) was used as an igniter to promote an exothermic reaction with higher-heat. The chemical reaction of the igniter is represented in reaction (2).

$$Fe_2O_{3(s)} + 2Al_{(s)} \rightarrow 2Fe_{(s)} + Al_2O_{3(s)};$$
$$T_{ad} = 3{,}088.4\ °C,\ \Delta H = -852.69\ kJ \cdot mol^{-1} \quad (2)$$

The reactant powders were weighed according to the required reaction stoichiometry for 10 g and dry milled for 2 h using a high-speed ball mill. A cylindrical graphite mold with a diameter of 25.4 mm was filled with the milled reactant mixture which was then a mechanically compacted to form a green reactant compact. Before the SHS reaction, a compacted igniter was put on the top of the green reactant compact.

2.3.1. Synthesizing under inert environment

The green reactant compact coupled with the igniter was

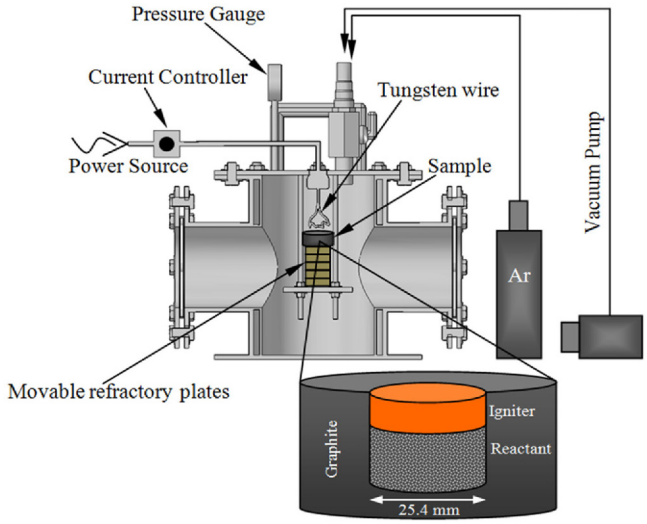

Fig. 1. Experimental set up under an inert environment. The inset shows a cross-section of the graphite mold containing the reactant compact and igniter.

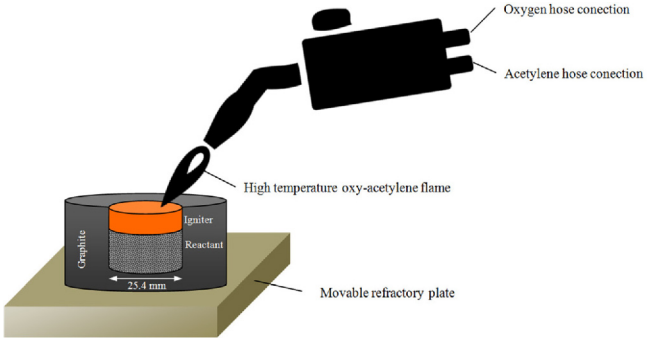

Fig. 2. Experimental set up under an air environment, inset shows a cross-section of the graphite mold.

loaded into the SHS reactor, which was preliminarily evacuated to remove all possible comtamination from atmospheric gases. Subsequently, static argon (Ar) was introduced to a pressure of 0.5 MPa (~4.95 atm). The combustion duration in Ar was approximately 15 s. The operation was always repeated at least twice to ensure an inert environment during the reaction cycle. This experiment used tungsten wire as an external heating source. The experimental apparatus is illustrated in Fig. 1.

2.3.2. Synthesizing under air environment

The experimental procedure schematically represented in Fig. 2 used an oxy-acetylene flame as the external heating source (the temperature of the oxy-acetylene flame was about 3,000 °C [23]) in an air environment (~1 atm or ~0.1 MPa).

SHS reaction was initiated by igniting the top of an igniter compact with an external heat source of either a tungsten wire or an oxy-acetylene flame. The high-exothermic heat generated by the igniter moved rapidly in a spiral wave-like mode downward from the top plane through the green reactant compact until it reacted the opposite end. The combustion duration in air was approximately 28 s.

After the reaction and cooling down to room temperature, the complete of combustion reaction can be observed closely by the decreasing of the glow intensity. The by-product (Fe and Al_2O_3) of the reaction (2) was able to simply break away from the synthesized product by hand. After igniting, Fe_2O_3 and Al were heated and melted. These compounds transferred heat to the reactants underneath it. However, there was no penetration happened during the heat transfer process as the solid of the compound could be collected after it was cooled down.

The as-synthesized products were mechanically pestled in a zirconia mortar into friable powders. In order to remove impurities and intermediete products, these powders were leached using solutions of HCl: CH_3COOH (v/ v) at 40 °C for 1 h, followed by HF: H_2O (v/ v) at 40 °C for 1 h under moderate stirring. The ratio of powdered product to leaching agent was 1.5 g : 60 mL throughout the experiment. After each leaching step, the leached product was filtered and washed with deionized water several times in order to adjust pH to 7.0 and finally dried at 100 °C. This procedure followed the work of Chanadee and Niyomwas [7].

2.3.3. Characterization of Si-SiC composite

The morphologies of the as-synthesized products and as-leached powders were characterized using scanning electron microscopy (SEM, Quanta 400, FEI, USA) coupled with energy dispersive X-ray (EDX, ISIS 300, Oxford, England) : their phase identifications were investigated by X-ray diffraction (XRD, X' Pert, MPD PHILIPS, the Natherland) which was operated with scan rate of $3°\cdot min^{-1}$ at 40 kV and current setting of 30 mA, and CuK_α radiation (1.5405 Å) was used. Fourier transform infrared (FT-IR) spectroscopy (Bruker, TENSOR 27, USA) recorded in a wavenumber range of 400-4000 cm^{-1} was used to determine the atomic bonding in as-leached product powders.

3. RESULTS AND DISCUSSION

3.1. Preparation of fly ash-based silica

XRF technique was used to evaluate the chemical composition of FA and FA-S. The results are presented in Table 1. The sum of SiO_2+Al_2O_3+Fe_2O_3 of FA-5 was 51.40%, thus it was classified as class C. FA-5 was selected as the preferred fly ash-based silica due to its high content of SiO_2 (81.48%). After leaching with HCl solution, unwanted metal oxides, including Al_2O_3, CaO, SO_3, Fe_2O_3, and other trace compounds were converted into soluble inorganic chloride compounds, expressed in the following possible chemical reactions [25]:

$$Al_2O_{3(s)} + 6HCl_{(aq)} \rightarrow 2AlCl_{3(aq)} + 3H_2O_{(l)} \quad (3)$$

$$CaO_{(s)} + 2HCl_{(aq)} \rightarrow CaCl_{2(aq)} + H_2O_{(l)} \quad (4)$$

Table 1. Chemical composition of FA and FA leached with different concentrations of HCl solution

Composition	Content (wt%)			
	FA	FA-1	FA-3	FA-5
Al_2O_3	9.73	12.43	5.20	1.43
BaO	-	-	0.29	0.19
CaO	31.98	20.09	4.32	1.61
Fe_2O_3	23.71	31.48	31.02	1.29
K_2O	2.02	2.41	0.62	0.42
MgO	2.17	1.59	1.63	-
MnO	0.34	0.55	-	-
Na_2O	1.49	-	-	-
SiO_2	17.96	22.62	37.18	81.48
SO_3	9.18	4.68	5.09	2.07
SrO	0.48	0.53	0.16	0.07
TiO_2	0.34	0.55	0.49	0.27
ZrO_2	-	-	0.07	0.06

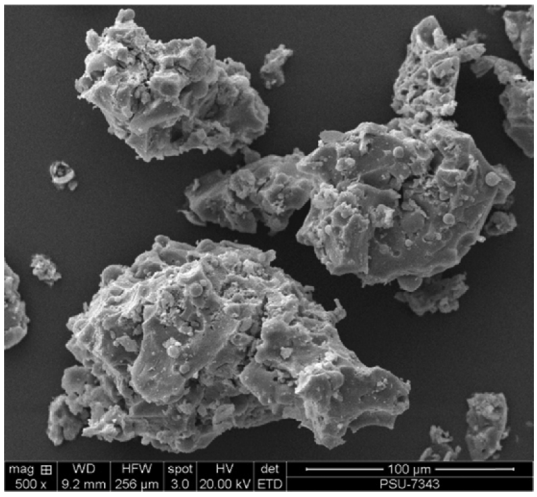

Fig. 3. SEM micro-photograph of FA-5.

$$SO_{3(s)} + 2HCl_{(aq)} \rightarrow SO_2Cl_{2(aq)} + H_2O_{(l)} \quad (5)$$
$$Fe_2O_{3(s)} + 6HCl_{(aq)} \rightarrow 2FeCl_{3(aq)} + 3H_2O_{(l)} \quad (6)$$

The morphology of FA-5 investigated by SEM is demonstrated in Fig. 3. It can be seen that the agglomerated FA-5 particles had an irregular shape with the size ranging from approximately 50 to 150 μm. The agglomeration and irregular shape of particles were due to inter-particle contact caused by surface covering with calcium [26].

3.2. Preparation of sawdust-based activated carbon

In the activation process, the reaction mechanisms between the activated agent K_2CO_3 and the carbonaceous materials (to enhance the chemical erosion of carbon) mainly took place as follows [27]:

$$K_2CO_{3(aq)} + 2C_{(s)} \rightarrow 2K_{(s)} + 3CO_{(g)} \quad (7)$$
$$K_2CO_{3(aq)} \rightarrow K_2O_{(s)} + CO_{2(g)} \quad (8)$$
$$K_2O_{(s)} + C_{(s)} \rightarrow 2K_{(s)} + CO_{(g)} \quad (9)$$

It was generally believed that part of the carbon is consumed according to reaction (7). In addition, the decomposition of K_2CO_3 gives rise to K_2O and CO_2, which were reduced by carbon to give K and CO (reaction (8)). The obtained K_2O would have further reacted with carbon in some active sites (reaction (9)) [28]. In addition, during the decomposition of SD at 500 °C, the volatile compounds containing mainly H, O, and N leave the carbonaceous structure and the SD becomes more predominantly carbon in composition.

Table 2 showed the results obtained for samples activated with K_2CO_3 under air atmosphere at different holding times (1-8 h) and constant activation temperature. The results revealed that the carbon content increased from 43.32% to 60.04% when the holding time was 3 h. At longer holding times, however, the carbon content decreased because the longer holding time would result in more carbon being burn-off and a carbon-CO_2 reaction (devolatilization process) would occur, as in previous research [29,30]. Since SD-3 contained more carbon than the other samples, it was chosen as the preferred sawdust-based activated carbon in accordance with the results in Table 2. The morphology of SD-3 investigated by SEM is depicted in Fig. 4. The image shows the presence of agglomeration and irregular plate-like particles. This agglomeration caused by the capillary force between micro-pores that arose in pyrolysis process [31].

3.3. Synthesis and characterization of Si-SiC composite powders

3.3.1. Formation mechanisms

Schubert and Hüsing [22] proposed that the formation reaction of SiC at high temperature (approximately 1,400 °C from phase diagram of Si-C binary system [32]) was initiated at a contact surface between solid SiO_2 and C. Afterward, the reaction was continuously driven by sub-reactions which transported mass through gaseous phases. The thermodynamics in terms of free energy (ΔG) are expressed in the reaction (10)-(13)

Table 2. Elemental analysis of SD and SD-based activated carbon at different holding times

Composition	Content (%)				
	SD	SD-1	SD-3	SD-5	SD-8
C	43.32	56.69	60.04	56.52	17.76
H	5.91	1.84	1.87	2.09	1.08
N	-	-	-	-	-
O (estimated by difference)	50.77	41.47	39.09	41.39	81.16

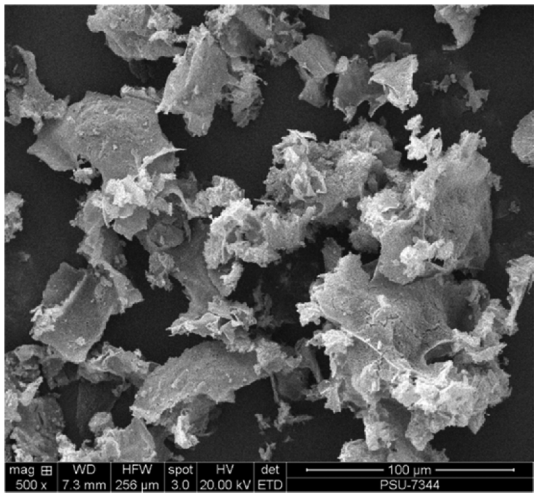

Fig. 4. SEM micro-photograph of SD-3.

which were shown in Fig. 5 as well.

$$SiO_{2(s)} + C_{(s)} \rightarrow SiO_{(g)} + CO_{(g)};\ \Delta G = 117.185\ kJ{\cdot}mol^{-1} \quad (10)$$
$$CO_{(g)} + SiO_{2(s)} \rightarrow SiO_{(g)} + CO_{2(g)};\ \Delta G = 237.917\ kJ{\cdot}mol^{-1} \quad (11)$$
$$CO_{2(g)} + C_{(s)} \rightarrow 2CO_{(g)};\ \Delta G = -120.732\ kJ{\cdot}mol^{-1} \quad (12)$$
$$SiO_{(g)} + 2C_{(s)} \rightarrow SiC_{(s)} + CO_{(g)};\ \Delta G = -77.709\ kJ{\cdot}mol^{-1} \quad (13)$$

when solid state reaction between SiO_2 and C occured, the gaseous of SiO and CO were released (reaction (10)). Then, CO gas reacted with the remaining solid of SiO_2 to form additional SiO and CO_2 gasses (reaction (11)). Although reactions (10) and (11) were not favorable in terms of energy calculations, Weimer [33] had confirmed that these reactions were still possible kinetically at high-temperatures. Subsequently, CO_2 gas was reversely transformed to CO gas by the reaction (12). After that, SiO gas directly reacted at the surface of C and Si diffused into C particle. Finally, SiC layer was formed, grew and encapsulated C core (reaction (13)). In addition, CO gasses released from reaction (10) and (12) can be reversely reacted with the remaining solid of SiO_2 and to form SiC.

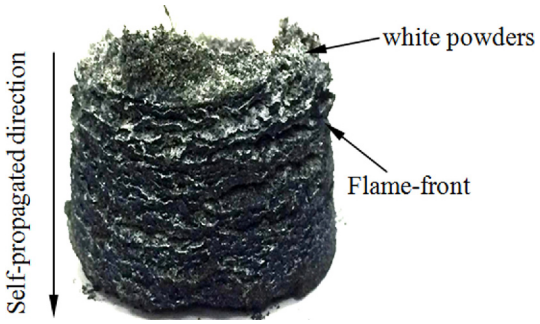

Fig. 6. Digital photograph of SHS product synthesized in Ar.

3.3.2. Physical characteristics

Figure 6 presents the physical characteristics of the SHS product synthesized under Ar atmosphere. The product exhibited flame-front layers with nearly parallel transverse channels through the self-propagated direction. This observation was typical for SHS synthesis involving gaseous phases (SiO, CO, CO_2 gases) [34].

The SHS product synthesized under atmospheric air is shown in Fig. 7. It can be seen that this reaction product was different from the product synthesized under Ar atmosphere. Synthesized under atmospheric air, the external pressure was not enough to suppress the high internal pressure from the reaction's heat, that was released along the layers of flame front resulting in the formation of the large channels in the as-synthesized product and the scattered reactant powders revealed in Fig. 7(a). Moreover, white powders were also observed on the surface of the products synthesized from both air and Ar (Figs. 7(a) and 7(b)). According to the research of Gadakary *et al*. [35], the white powders were MgO. Their results were confirmed by the appearence of Mg and oxygen spectra from the EDX analysis.

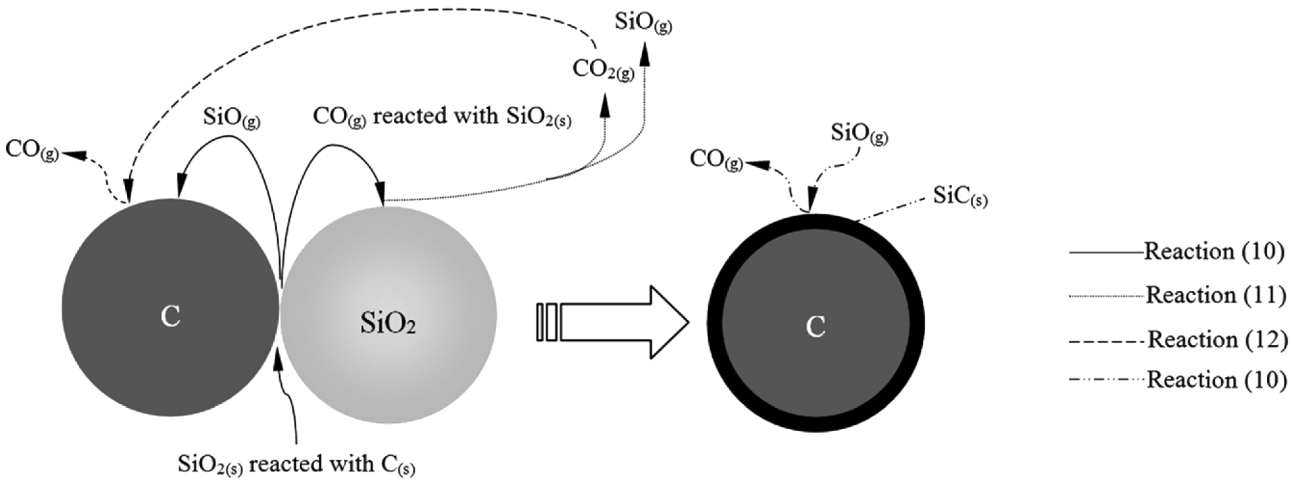

Fig. 5. Schematic represented the reaction mechanisms to form SiC in this study.

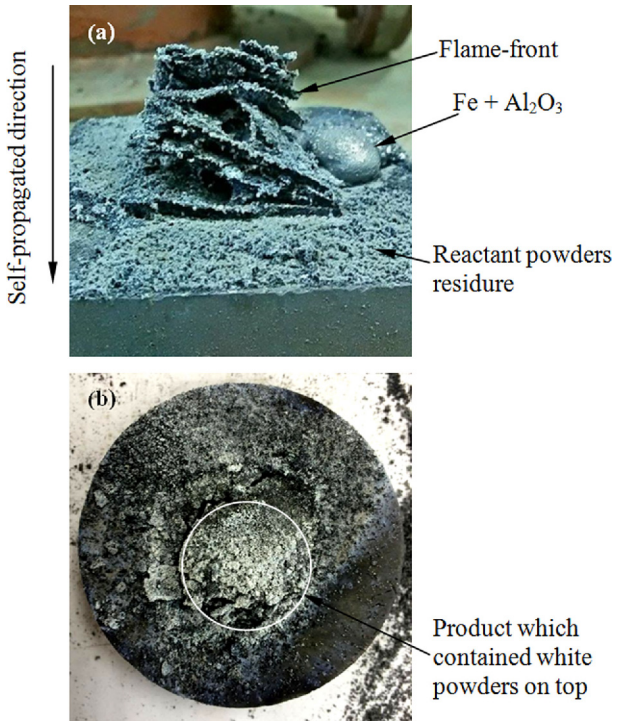

Fig. 7. Digital photograph of SHS product synthesized in air. (a) side-view, outside graphite mold and (b) top-view, inside graphite mold.

As the flame-front propagated, the exothermic heat generated by the SHS reaction could dissipate to sinks around the sample, consuming reaction heat required for the complete phase transformation to the final product [21].

3.3.3. Phases identification

XRD patterns obtained from the SHS combustion products synthesized in both experimental atmospheric environments are shown in Fig. 8 and XRD patterns obtained from the leached products are shown in Fig. 9. Also, the comparative phase compositions of the as-synthesized and as-leached products calculated by a semi-quantitative method [36] can be seen in Table 3.

The results in Fig. 8(a) shows that the SHS product synthesized under air consisted of Si ($2\theta \cong 28.46°$, ICDD no. 03-065-1060), SiC ($2\theta \cong 35.65°$, ICDD no. 01-075-0254), a by-product, MgO ($2\theta \cong 42.88°$, ICDD no. 01-087-0651), unstable phases of Mg_2Si ($2\theta \cong 40.05°$, ICDD no. 01-077-9648), and Mg_2SiO_4 ($2\theta \cong 22.84°$, ICDD no. 01-076-0851), and unreacted phases of Mg ($2\theta \cong 68.59°$, ICDD no. 01-080-4430) and SiO_2 ($2\theta \cong 21.86°$, ICDD no. 01-076-0939). In Fig. 8(b) they show that the SHS product synthesized under Ar consisted of Si, SiC, a by-product (MgO) and only one unstable phase (Mg_2SiO_4).

The presence of unstable Mg_2SiO_4 and Mg_2Si in the XRD patterns of the SHS products in Figs. 8(a) and 8(b) may be due to an incomplete conversion caused by the fast cooling rate of

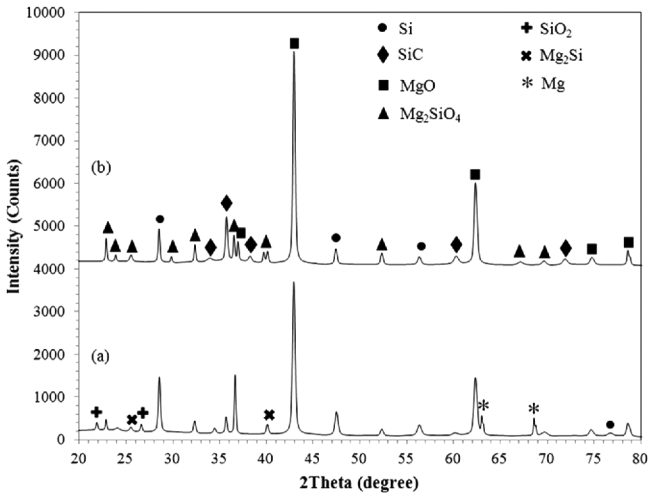

Fig. 8. XRD patterns of the SHS products synthesized in different atmospheres (a) air and (b) Ar.

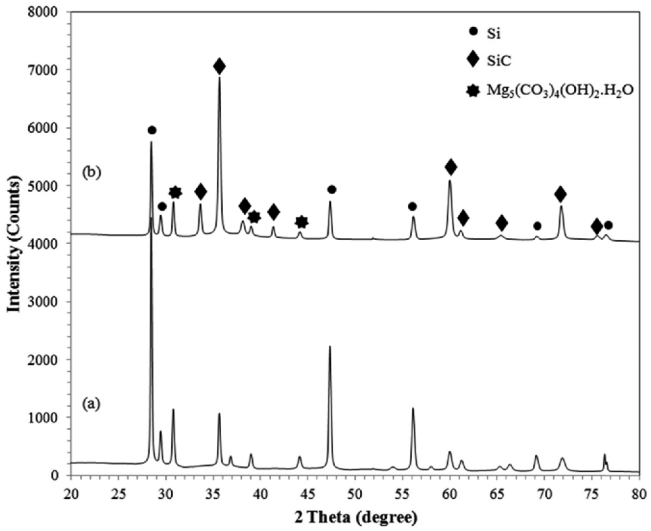

Fig. 9. XRD patterns of the SHS products synthesized in different atmospheres (a) air and (b) Ar, after two leaching steps.

the reaction [7]. In particular, the presence of unstable Mg_2SiO_4 in both SHS products might be due to the production of gas phase products such as Mg (g) and SiO (g) which, at high temperature during an SHS reaction, could react at a pressure below 10 atm (~1 MPa), leading to the formation of Mg_2SiO_4 [34,37]. Moreover, it was found that the SHS product synthesized under air contained more Mg_2SiO_4 than the SHS product synthesized under Ar (see Table 3).

The unreacted SiO_2 found in the SHS product synthesized under atmospheric air (Fig. 8(a)) due to the oxidation reaction of free silicon (Si) left over from the reaction between SiO_2 and C [5]. This is the most important factor preventing the required conversion for the formation of SiC, so the amount of SiC in the SHS product synthesized under air was lower than under an Ar atmosphere (see Table 3). In addition, from

Table 3. Comparison of the phase composition of as-synthesized and as-leached products

Atmospheric environment	Composition (wt%)							
	Si	SiC	MgO	Mg_2SiO_4	Mg_2Si	SiO_2	Mg	$Mg_5(CO_3)_4(OH)_2.4H_2O$
	As-synthesized products							
Air	15.72	16.63	50.67	1.11	2.21	3.89	9.77	-
Ar	12.46	17.22	69.52	0.80	-	-	-	-
	As-leached products							
Air	72.68	14.72	-	-	-	-	-	12.51
Ar	36.35	53.31	-	-	-	-	-	10.34

the mass balance, the calculated degree of Si transformed from a starting FA-5 into Si containg in final SiC (leached products) indicated the SiC yield synthesized in air (11.99%) was lower than the SiC yield synthesized in Ar (43.44%). However, in Fig. 8(a), the unreacted Mg was found in the SHS product synthesized under atmospheric air probably due to the uncomplete reaction in some part of the reactant compact.

XRD patterns in Figs. 9(a) and 9(b) indicated that Si and SiC were major phases of as-leached-SHS products. Furthermore, residual phases called hydromagnesite ($Mg_5(CO_3)_4(OH)_2.4H_2O$) ($2\theta \approx 30.77°$, ICDD no. 01-070-0361) were present in the XRD patterns of both as-leached-SHS products. It is probable that these hydromagnesites were precipitated in the 2nd leaching step with HCl: CH_3COOH solution. Because the MgO was not completely removed from the product by HCl solution in the 1st leaching step, the residual MgO further reacted with the carboxyl group (-COOH) in acetic acid and nucleated into magnesium carbonate hydrate ($MgCO_3 \cdot H_2O$). Gradually, crystals of $Mg_5(CO_3)_4(OH)_2 \cdot 4H_2O$ were formed [38].

A representative IR transmittance spectrum of the as-leached product powders at different synthesis atmospheres are shown in Fig. 10. As-leached products both in air and Ar revealed broad peaks at 3600-3300 cm^{-1} are attributed to O-H vibration of bridging oxygen in water molecule. The peaks at 1643 cm^{-1} correspond to C-C stretching vibration. The bands at 1049-990 cm^{-1} are the O-H bending mode associated with bicarbonate. Furthermore, the bands ranges from 750 to 500 cm^{-1} are the absorption peaks of the Mg-O-Mg bond. Thus, it can be concluded that the as-leached product powders contained $Mg_5(CO_3)_4(OH)_2 \cdot 4H_2O$ [39,40]. The FT-IR results are consistent with the XRD results (Figs. 9(a) and 9(b)). In addition, the peaks at 828 cm^{-1} are attributed to Si-C stretching vibration implying the generation of SiC [40]. Note that, in Ar synthesis system, the O-H band and Mg-O-Mg band were weak whereas the signal of Si-C band was strong. This indicated that less $Mg_5(CO_3)_4(OH)_2 \cdot 4H_2O$ and more SiC were produced. The results are consistent with the XRD-semiquantitative (Table 3).

3.3.4. Microstructures and morphologies

Figure 11 presents SEM images of as-synthesized product particles, (a), (b) and as-leached product particles, (c), (d). Prior to the leaching process, the product revealed agglomerated

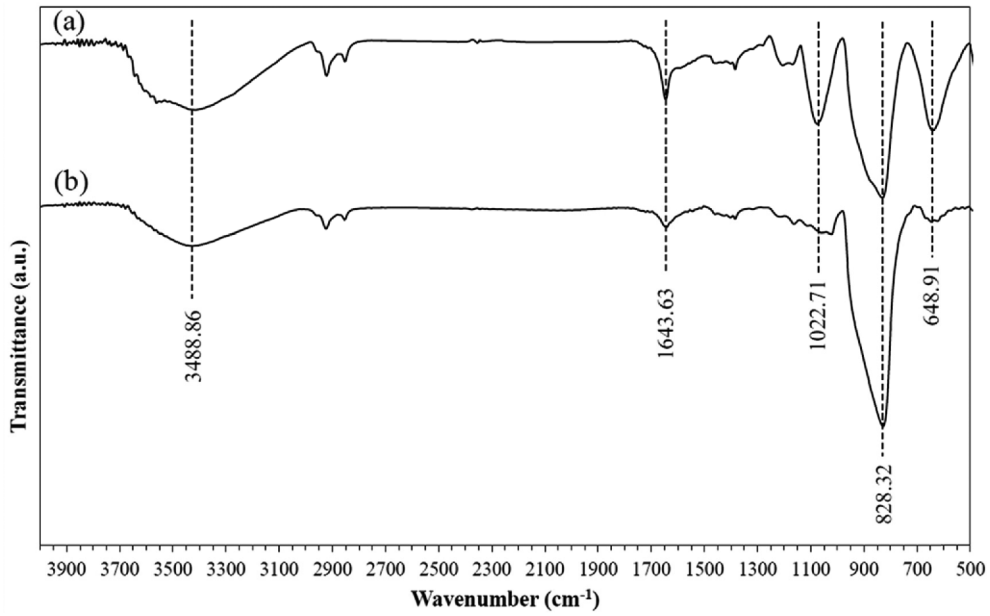

Fig. 10. FT-IR spectra of the SHS products synthesized in different atmospheres (a) air and (b) Ar, after two leaching steps.

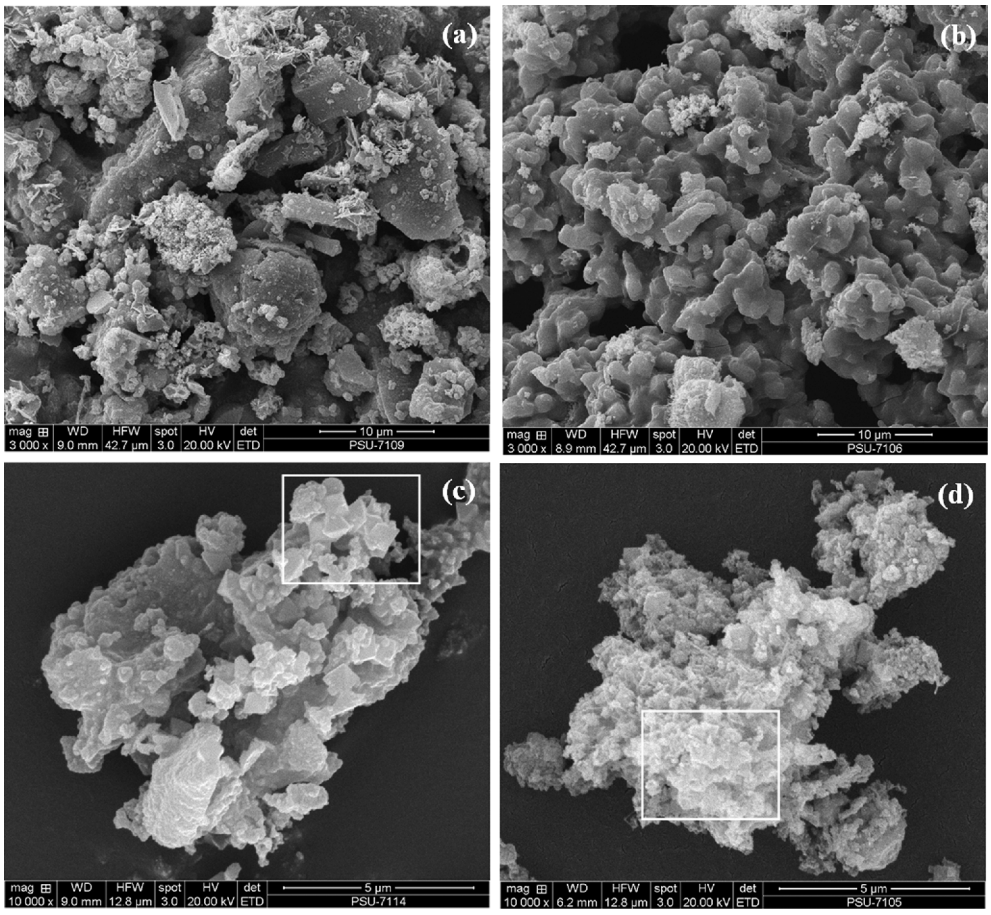

Fig. 11. SEM micrographs of the SHS product powders from FA-5/SD-3/Mg synthesized (a) in air, and (b) in Ar and as-SHS product synthesized (c) in air, and (d) in Ar, after two leaching steps.

particles which included distinct phases. The leached product particles seen Figs. 11(c) and 11(d) appear to be finer, homogeneous and smaller than 5 μm (see inset). Moreover, it can be seen that both the as-synthesized and as-leached product particles reacted under Ar atmosphere were smaller than those synthesized under atmospheric air.

The synthesis atmosphere had an effect on the size of the product particles. Major parameters that control the crystallization and particle growth-rate in SHS reactions are growth-time and cooling rate. Under Ar, both fast propagation and fast cooling rate were accomplished, and nucleated-particles did not have enough time to develop, therefore, smaller of product particles were obtained [41].

Arrived at by the Scherrer equation [42], calculations of the crystalline size of leached-SHS product particles are shown in Table 4. It can be observed that the crystalline size of as-leached-SHS product synthesized in Ar (39.48 nm) to be smaller than those synthesized in air (51.16 nm).

The SEM micrograph in Fig. 12 displayed particles of Si-SiC composite synthesized from FA-5/SD-3/Mg under Ar atmosphere after the leaching process: supporting EDX micro-analysis data is shown alongside.

Table 4. Crystalline size of Si-SiC composite powder synthesized by SHS in experimental atmospheres after leaching

Atmospheric environment	Crystalline size (nm)		
	Si	SiC	Average
Air	58.02	44.30	51.16
Ar	43.51	35.45	39.48

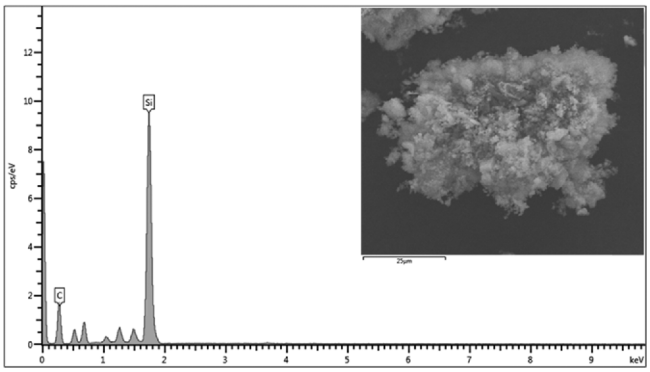

Fig. 12. SEM-EDX spectra of Si-SiC composite powders synthesized from FA-5/SD-3/Mg by SHS in Ar after leaching process (oxygen and trace elements were not quantified).

4. CONCLUSION

In this work, Si-SiC composite powders were produced by leaching out impurities from SHS combustion products that were successfully synthesized from reactants of fly ash-based silica prepared from coal mining fly ash, sawdust-based activated carbon prepared from Para rubber-wood sawdust, and Mg metal (optimized as FA-5/SD-3/Mg). The SHS product was low in impurities, had a high Si to SiC content (36.35 wt%Si, 53.31 wt%SiC), and a small average crystalline size (39.48 nm) was achieved using Ar as the synthesis atmosphere. The industrial waste materials used, coal mining fly ash and Para rubber-wood sawdust, could be effective and inexpensive reactants for obtaining low-cost Si-SiC composite powders.

ACKNOWLEDGEMENT

The author would like to thank Miss Rosita Sondee, a B. Sc student in the Materials Science Program for her valuable help in carrying out some experiments and especially Assoc. Prof. Dr. Sutham Niyomwas for his assistance with the SHS reactor and oxy-acetylene flame torch. The author would also like to acknowledge Mr. Thomas Duncan Coyne for corrections and improvements to the English text.

REFERENCES

1. Z. Károly, I. Mohai, S. Klébert, A. Keszler, I. Sajó, and J. Szépvölgyi, *Powder. Technol*. **214**, 300 (2011).
2. H. Zhang, W. Ding, K. He, and M. Li, *Nanoscale. Res. Lett*. **5**, 1264 (2010).
3. S. Bhaumik, C. Divakar, S. Devi, and A. Singh, *J. Mater. Res*. **14**, 906 (1999).
4. S. Niyomwas, *JMMM*. **19**, 21 (2009).
5. Y. Yang, Z. Lin, and J. Li, *J. Eur. Ceram. Soc*. **29**, 175 (2009).
6. R. Mahmoodian, R. Yahya, A. Dabbagh, M. Hamdi, and M. Hassan, *PLoS. One*. **10**, 1 (2015).
7. T. Chanadee and S. Niyomwas, *Key. Eng. Mat.* **675-676**, 623 (2016).
8. L. Zhang, X. Wang, and J. Yang, *Appl. Mech. Mater.* **152-154**, 589 (2012).
9. Y. Yin, B. Ma, S. Li, B. Zhang, J. Yu, Z. Zhang, *et al. Ceram. Int*. **42**, 19225 (2016).
10. A. Dey and K. Pandey, *Rev. Adv. Mater. Sci*. **44**, 168 (2016).
11. Sulardjaka, Jamasri, M. W. Wilda, and Kusnanto, *B. Mater. Sci*. **34**, 1013 (2011).
12. H. Cui, Y. Zheng, J. Ma, S. Yang, G. Tian, X. Liu, *et al. J. Wood. Sci*. **63**, 95 (2017).
13. Y. Chiew and K. Cheong, *Mater. Sci. Eng. B* **176**, 951 (2011).
14. V. Karelin, A. Strashko, A. Sazonov, and A. Dubrovin, *Resource-Efficient Technologies* **2**, 50 (2016).
15. C. Srinivasakannan and M. Bakar, *Biomass Bioenerg* **27**, 89 (2004).
16. C. Bouchelta, M. Medjram, O. Bertrand, and J. Bellat, *J. Anal. Appl. Pyrol*. **82**, 70 (2008).
17. G. Couto, A. Dessimoni, M. Bianchi, D. Perígolo, and P. Trugilho, *Ciênc. Agrotec*. **36**, 69 (2012).
18. S. Niyomwas, *Properties and Applications of Silicon* (ed. R. Gerhardt), p. 411, InTech, Croatia (2011).
19. M. Dehghanzadeh, A. Ataie, and S. Manesh, *Int. J. Mod. Phys.* **5**, 263 (2012).
20. R. Andrievski, *Rev. Adv. Mater. Sci*. **22**, 1 (2009).
21. J. Moore and H. Feng, *Prog. Mater. Sci*. **39**, 243 (1995).
22. U. Schubert and N. Hüsing, *Synthesis of Inorganic Materials*, pp.22-26, WileyVCH, Weinheim, Germany (2012).
23. L. Zeatoun and P. Morrison, *J. Mater. Res*. **12**, 1237 (1997).
24. L. Ibrahim, *Water. Sci*. **29**, 109 (2015).
25. L. Cui, Y. Guo, X. Wang, Z. Du, and F. Cheng, *Chiness. J. Chem. Eng*. **23**, 590 (2015).
26. B. Kutchko and A. Kim, *Fuel* **85**, 2537 (2006).
27. C. Lu, S. Xu, and C. Liu, *J. Anal. Appl. Pyrol*. **87**, 282 (2010).
28. J. Zhang, Z. Zhong, J. Zhao, M. Yang, W. Li, and H. Zhang, *Can. J. Chem. Eng*. **90**, 762 (2012).
29. Y. Chen, B. Huang, M. Huang, and B. Cai, *J. Taiwan. Inst. Chem. E*. **42**, 837 (2011).
30. X. Jin, Z. Yu, and Y. Wu, *Cell. Chem. Technol*. **46**, 79 (2012).
31. W. Ghani, A. Mohd, G. Silva, R. Bachmann, Y. Taufiq-Yap, U. Rashid, and A. Muhtaseb, *Ind. Crops. Prod*. **44**, 18 (2013).
32. L. Sadler and M. Shamsuzzoha, *J. Mater. Res*. **22**, 147 (1997).
33. A. Weimer, *Carbide, Nitride and Boride Materials Synthesis and Processing*, pp.94-96, Springer Science & Business Media, London, UK (2012).
34. A. Mukasyan, *Properties and Applications of Silicon* (ed. R. Gerhardt), p. 389, InTech, Croatia (2011).
35. S. Gadakary, M. Davidson, R. Veerababu, and A. Khanra, *J. Min. Metall. Sect. B-Metall*. **52**, 69 (2016).
36. J. Ramos, J. Hernández, A. Cambeses, J. Scarrow, and A. Galindo, *An Introduction to the Study of Mineralogy* (ed. C. Aydinalp), p. 73, InTech, Croatia (2012).
37. Z. Yermekova, Z. Mansurov and A. Mukasyan, *Int. J. Self-Propag. High-Temp. Synth*. **19**, 96 (2010).
38. A. Sanna, M. Uibu, G. Caramanna, R. Kuusik, and M. Valer, *Chem. Soc. Rev*. **43**, 8049 (2014).
39. W. Yin, Y. Wang, Q. Ji. Yao, Y. Hou, L. Wang, and W. Zhong, *Int. J. Miner. Metall. Mater.* **21**, 304 (2014).
40. Z. Li, T. Shi, and D. Tan, *J. Serb. Chem. Soc*. **78**, 1213 (2013).
41. S. Ko, C. Won, and I. Shon, *Scripta Mater*. **37**, 889 (1997).
42. H. Jin, J. Li, M. Cao, and S. Agathopoulos, *Powder Technol*. **196**, 229 (2009).